Available online at www.sciencedirect.com
ScienceDirect
International Journal of Thermal Sciences 47 (2008) 157–174
International Journal of Thermal Sciences
www.elsevier.com/locate/ijts

Two-dimensional coal combustion modeling of CFB

Afsin Gungor *, Nurdil Eskin

Istanbul Technical University, Mechanical Engineering Faculty, Gumussuyu, 34437, Istanbul, Turkey

Received 17 March 2006; received in revised form 8 December 2006; accepted 10 January 2007

Available online 23 February 2007

Abstract

In this study, a dynamic 2D model for a CFB combustor has been developed which integrates and simultaneously predicts the hydrodynamics, heat transfer and combustion aspects. Hydrodynamic model used in this study has been developed in our previous studies. Simulation model calculates the axial and radial distribution of voidage, velocity, particle size distribution, pressure drop, gas emissions and temperature at each time interval for gas and solid phase both for dense bed and for riser. The model has been validated against the data from a pilot-scale 50 kW CFB combustor and an industrial-scale 160 MW CFB combustor. A sensitivity analysis is carried out using the model to examine the effect of different operational parameters and coal properties on bed temperature and the overall CO, NO_x and SO_2 emissions from the combustor. As a result of parametric study, it is observed that by increasing bed operational velocity or excess air ratio, bed temperature decreases and CO emission increases. Bed operational velocity has a more significant effect on CO emission than to bed temperature. Another effect of increasing excess air is the decrease of SO_2 and NO_x emissions. However, NO_x emission increases with the operational bed velocity while SO_2 emission decreases.

Keywords: Circulating fluidized bed; Modeling; Coal combustion

1. Introduction

The use of fluidized bed equipment has opened wide possibilities for ensuring reliable design and improving various industrial technologies, such as: coal combustion, gasification and drying. Operating either in the fast fluidization regime or in the transported bed regime, the circulating fluidized bed (CFB) riser reactor has many advantages over the conventional bubbling or turbulent fluidized bed reactors, such as the ability to burn a wide variety of solid fuels with low pollutant emissions, high combustion efficiency, having smaller combustor cross-section, fewer feed points, good turndown and load capability.

The main goal of the modeling of CFB combustors is to constitute a system that maximizes combustion efficiency, and minimizes operating and investment costs and air pollutant emissions. It is also important to determine the effects of operational parameters in CFB combustors via simulation study instead of expensive and time-consuming experimental studies. Designing of the CFB combustor is very important because of burning coal with high efficiency and within acceptable levels of gaseous emissions. A good understanding of the combustion and pollutant generating processes in the combustor can greatly avoid costly upsets. The modeling has been dealt with in a number of efforts by either 1D, 1.5D, 2D or 3D approaches. The publications in the literature about the CFB modeling may also be subdivided into those that consider the hydrodynamic behavior [1–10], and the others that investigate the combustion phenomena [11–21].

Investigations about the CFB modeling that consider the hydrodynamic behavior have been carried out by many different researchers in the literature. Harris and Davidson [1] classified all models in three broad groups: *Type I*: models that predict the axial variation of solids holdup, but not the radial one (simple axial solids distribution models) [2]. *Type II*: models that predict the axial and the radial variation of solids holdup by assuming two or more phases, e.g., a core/annulus or clustering approach (core/annulus models) [3]. *Type III*: models that employ fundamental equations of fluid dynamics to predict two phase gas/solid flow. They are based on gas and solid phase continuity equations, momentum balances and the appropriate constitutive equations (CFD models) [4–8]. Models of type III

* Corresponding author. Tel.: +90 505 504 49 02; fax: +90 212 245 07 95.
E-mail address: afsingungor@hotmail.com (A. Gungor).

1290-0729/$ – see front matter
doi:10.1016/j.ijthermalsci.2007.01.017

Nomenclature

Ar	Archimedes number	
C	gas concentration	$\mathrm{kmol\,m^{-3}}$
Ca/S	calcium to sulphur ratio	
C_D	drag coefficient	
c_p	specific heat of solids	$\mathrm{kJ\,kg^{-1}\,K^{-1}}$
c_v	specific heat of gas	$\mathrm{kJ\,kmol^{-1}\,K^{-1}}$
D	bed diameter	m
D_b	Equivalent bubble diameter	m
D_g	diffusivity coefficient for oxygen in nitrogen	$\mathrm{m^2\,s^{-1}}$
d	diameter	m
d_p	particle diameter	m
d_{pi}	particle dimension interval	m
$d_{p,\mathrm{new}}$	particle diameter after fragmentation	m
$d_{p,\mathrm{old}}$	particle diameter before fragmentation	m
EA	excess air	
f	wall friction coefficient	
G	solid stress modulus	$\mathrm{N\,m^{-2}}$
g	gravity	$\mathrm{m\,s^{-2}}$
H_b	combustor height	m
H_{bot}	height of the bottom zone	m
H_{upp}	height above the bottom zone	m
h	overall bed to wall heat transfer coefficient	$\mathrm{W\,m^{-2}\,K^{-1}}$
h_c	convection heat transfer coefficient for clusters	$\mathrm{W\,m^{-2}\,K^{-1}}$
h_d	convection heat transfer coefficient for dispersed phase	$\mathrm{W\,m^{-2}\,K^{-1}}$
h_{rc}	radiative heat transfer coefficient for clusters	$\mathrm{W\,m^{-2}\,K^{-1}}$
h_{rd}	radiative heat transfer coefficient for dispersed phase	$\mathrm{W\,m^{-2}\,K^{-1}}$
h_i	height above the distributor	m
$\dot{J}$	mass transfer rate via density difference per unit volume	$\mathrm{kmol\,m^{-3}\,s^{-1}}$
k	rate constant	$\mathrm{m\,s^{-1}}$
k_a	attrition constant	
k_{be}	mass transfer coefficient	$\mathrm{s^{-1}}$
k_c	char combustion reaction rate	$\mathrm{kg\,s^{-1}}$
k_{cr}	kinetic rate	$\mathrm{s^{-1}}$
k_{cd}	diffusion rate	$\mathrm{s^{-1}}$
k_f	fragmentation coefficient	
k_g	gas conduction heat transfer coefficient	$\mathrm{W\,m^{-1}\,K^{-1}}$
k_L	reaction rate	$\mathrm{s^{-1}}$
k_{vL}	volumetric reaction rate	$\mathrm{kg\,m^{-2}\,s^{-1}}$
M	molecular weight	$\mathrm{kg\,mol^{-1}}$
$\dot{m}$	mass flow rate	$\mathrm{kg\,s^{-1}}$
m_f	feed rate	$\mathrm{kg\,h^{-1}}$
N	number of particles in each control volume	
$\dot{n}$	gas flow rate	$\mathrm{mol\,s^{-1}}$
P	pressure	Pa
P_{acc}	acceleration component of pressure drop	
$P(d)$	particle size distribution function	
R	reaction rate	$\mathrm{mol\,s^{-1}}$, $\mathrm{mol\,cm^{-3}\,s^{-1}}$
$\dot{R}$	mass flow rate generated/consumed from chemical processes per unit volume	$\mathrm{kmol\,m^{-3}\,s^{-1}}$
R'''	total heat generated/consumed per unit volume	$\mathrm{W\,m^{-3}}$
R_a	particle attrition rate	$\mathrm{kg\,s^{-1}}$
R_b	bed radius	m
Re	Reynolds number	
R_u	Universal gas constant	$\mathrm{kJ\,mol^{-1}\,K^{-1}}$
R_g	gas constant	$\mathrm{kJ\,mol^{-1}\,K^{-1}}$
r	radial distance from riser axis	m
Sc	Schmidt number	
S_g	Specific surface area of limestone particles	$\mathrm{m^2\,kg^{-1}}$
Sh	Sherwood number	
T	temperature	K
T_{mean}	mean bed temperature	K
U_0	superficial velocity	$\mathrm{m\,s^{-1}}$
U_{mf}	minimum fluidization velocity	$\mathrm{m\,s^{-1}}$
u	gas velocity	$\mathrm{m\,s^{-1}}$
V	volatile yield	
V_g	volume of gas per kg of fuel	$\mathrm{m^3\,kg^{-1}}$
VM	volatile matter fraction, kg volatile	$(\mathrm{kg\,char})^{-1}$
v	particle velocity	$\mathrm{m\,s^{-1}}$
W_b	mass of particle	kg
X_k	char mass fraction, kg-char	$(\mathrm{kg\text{-}bed\ material})^{-1}$
x_a	weight fraction of particles after attrition at d_{pi} interval	
x_i	weight fraction of particles at d_{pi} interval	
y	mass fraction of gas species, kg-gas species	$(\mathrm{kg\text{-}gas})^{-1}$
Z_0	Bed characteristic height	m
z	Distance from top of the riser	m
z_i	Height of inflection point	m

Subscripts

b	bed
c	carbon
g	gas
j	gas–solid species
mf	minimum fluidization
p	particle
s	solid

Greek letters

β	gas–solid friction coefficient	
β'	constant defined in Eq. (6)	
δ	thickness of annulus	m
ε	void fraction	
ε_b	bubble volume fraction	
Φ	mechanism factor	
λ_s	limestone reactivity	
μ	gas viscosity	$\mathrm{kg\,m^{-1}\,s^{-1}}$
ρ	particle density	$\mathrm{kg\,m^{-3}}$
τ	shear stress	$\mathrm{N\,m^{-2}}$

are the most general and can deal with different geometries, but are numerically complex. Recently, van Wachem et al. [9] have given a comparative analysis of CFD models.

Basu [10] presented a comprehensive review of combustion of coal in CFBs. In that study coal combustion models are grouped under three levels of details of sophistication: *Level I*: The simplest model is 1D with plug flow reactor, where solids are back-mixed [11–13]. The 1D models do not consider the solid flow in the annular region of the riser, where temperature, gas concentration and velocity can differ from that in the core, in which an up-flowing dilute region is considered. *Level II*: Core-annulus, 1.5D, with broad consideration of combustion and other related processes [14–18]. *Level III*: 3D model based on Navier–Stokes equation [19–21]. The model of Hyppanen et al. [20], Tsuo et al. [21] used coarse grids and used macroscopic averaging procedure for aggregate properties of the cells. Some of the model parameters were evaluated by experiments [20]. This practice based 3D model analysis on both combustion and pollutant generation in a CFB [21].

In addition to these publications, numerous experimental and theoretical studies about gaseous emissions in CFB combustors are present in the literature [15,22–38]. Nitrogen oxides are a major environmental pollutant resulting from combustion. The reactions of nitrogen oxides with carbons or chars are of current interest with regard to their possible role in reducing NO_x emissions from combustion systems. They also offer new useful insights into the oxidation reactions of carbons, generally [22]. A large literature concerning these reactions has developed, as evidenced in three reviews [23–25] and by the recent publication of many papers in the area [26–36]. These works have suggested considerable complexity in the mechanisms of NO_x reduction and a large variability in reported kinetics. There are two approaches to describe NO_x emission in CFB [32]. The first approach involves overall reaction (considering catalytic activity of CaO and char). The overall rate constants are measured preferably under CFB conditions [33]. The other approach is more thorough, and is based on actual chemical reactions whose rate constants can be taken from literature [34]. For CFB only 106 reactions with 28 species were used to model the NO_x emission. However, a detailed review shows that all N-related reactions have not the same importance [35]. So instead of considering all N-related reactions, one could use only the important reactions for the development of a predictive procedure for the overall NO_x emission from a CFB combustor.

Circulating fluidized bed coal combustion with sorbent addition allows clean combustion of coals of different rank even with high sulfur and ash contents. Numerous experimental and theoretical studies about the sulfur retention in CFB combustors are present in the literature [15,27,37,38]. Some models have already been proposed for predicting the sulfur retention in CFB combustor, but there are important differences between their submodels, especially as far as the CFB hydrodynamics is considered [15,27,37,38].

In the present study, a dynamic two-dimensional model for a coal fired CFB combustor has been developed. Because coal combustion in a CFB combustor directly is affected by its hydrodynamic parameters, both hydrodynamic and combustion models are treated simultaneously to yield a predictive model for the CFB combustor. Hydrodynamic model used in this study has been developed in our previous studies [39,40]. Hydrodynamic model considers the bottom zone in turbulent fluidization regime as two-phase flow in detail which constitutes a major difference from most of the previous studies in the literature and the upper zone as having core-annulus solids flow structure. Hydrodynamic model calculates the axial and radial distribution of voidage and velocity for gas and solid phase, pressure drop for gas phase and solids volume fraction and particle size distribution for solid phase and has been validated against experimental results obtained from various CFB test rigs at different size in the literature. The model compares with experimental results for void fraction, solids volume fraction, and particle velocity along the bed height and bed radius and different bed operational parameters prove the model hydrodynamic structure validation axially and radially. Additionally inward solids mass flux along the bed radius and pressure gradient along the bed height is validated.

In the present study developed dynamic 2D model for a CFB combustor integrates and simultaneously predicts the hydrodynamics, heat transfer and combustion aspects. Simulation model calculates the axial and radial distribution of voidage, velocity, particle size distribution, pressure drop, gas emissions and temperature at each time interval for gas and solid phase both for dense bed and for riser. The model has been validated against the data from the 50 kW pilot CFB combustor using Tuncbilek lignite at the Gazi University Heat Power Laboratory and an industrial-scale 160 MW CFB combustor using Can lignite at Can Power Plant, obtained during the commissioning period [41,42]. A sensitivity analysis is carried out using the model to examine the effect of different operational parameters and coal properties on bed temperature and the overall CO, NO_x and SO_2 emissions from the combustor.

2. Model description

A very good appreciation of the combustion and pollutant generating processes is needed for a reliable performance prediction through modeling and can greatly avoid costly upsets. The present CFB combustor model can be divided into three major parts: a sub-model of the gas–solid flow structure; a reaction kinetic model for local combustion and a convection/dispersion model with reaction. The scheme of the CFB used in the model is shown in Fig. 1.

2.1. Hydrodynamics structure

Hydrodynamics plays a crucial role in defining the performance of CFBs. The flow structure of CFBs is known to exhibit axial nonuniformities [12]. In order to characterize this behavior, the riser is subdivided vertically into zones with different properties. According to the axial solid volume concentration profile, the riser is axially divided into two different zones: The bottom zone and the upper zone. There are great differences

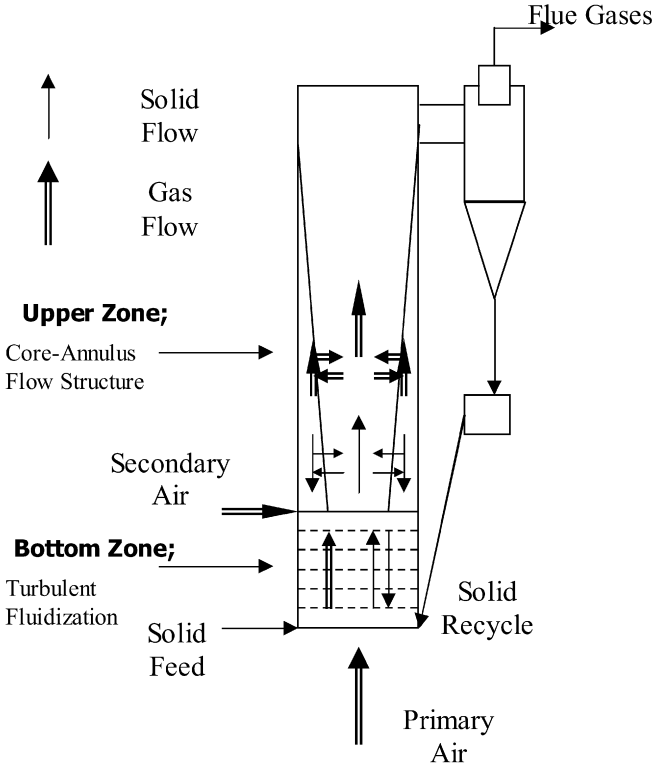

Fig. 1. The scheme of the CFB.

in the hydrodynamics between the bottom zone and the upper zone.

Svensson et al. [43], and Werther and Wein [44]'s experimental studies report that the fluid-dynamical behavior of the bottom zone is similar to that of bubbling fluidized beds. Furthermore, the results of studies carried out by Leckner et al. [45] and Montat et al. [46] imply that the combustion of coal, particles mixing and heat transfer in the dense bed dominate the performances of CFB. This implies that, bottom zone should be modeled in detail as two-phase flow. However, most of the models in the literature do not completely take account of the performance of the bottom zone, consider the bottom zone as well-mixed distributed flow with constant voidage, and use generally lumped formulation [1–13,15–38]. In the present study, bottom zone is modeled as two-phase flow which is subdivided into a solid-free bubble phase and a solid-laden emulsion phase [40,47]. The bubble rise velocity, the bubble size, the bubble volume fraction and the suspension porosity is calculated by Horio [48]. A single-phase back-flow cell model is used to represent the solid mixing in the bottom zone. Solids exchange, between the bubble and the emulsion phases is a function of the bubble diameter and varies along the axis of the riser and it is considered in the model as follows [49]:

$$k_{be,s} = \frac{3(1-\varepsilon_{mf})U_{mf}}{(1-\varepsilon_b)\varepsilon_{mf} D_b} \tag{1}$$

where D_b is the bubble diameter predicted by a correlation established by Mori and Wen [50]. In the model, gas interchange coefficient is considered as follows [51]:

$$k_{be,g} = \frac{11}{D_b} \tag{2}$$

In the model, the minimum fluidization velocity is obtained according to Wen and Yu [52]:

$$U_{mf} = \frac{\mu}{C d_p}\left[(33.7^2 + 0.0651Ar)^{0.8} - 33.7\right] \tag{3}$$

where C is the gas mixture concentration in the control volume. Minimum fluidization voidage (ε_{mf}) is taken as 0.5 in the model calculations [42]. Between the bottom zone and the riser exit the upper zone is located. For the upper zone, core-annulus flow structure is used [2]. Particles move upward in the core and downward in the annulus. Thickness of the annulus varies according to the bed height. δ is given by Werther and Wein [44] as

$$\frac{\delta}{D} = 0.55 \cdot Re^{-0.22}\left(\frac{H_b}{D}\right)^{0.21}\left(\frac{H_b - h_i}{H_b}\right)^{0.73} \tag{4}$$

Smolders and Baeyens [2] proposed a model in which the bed density was described as an exponential function of the bed height. In this paper, the model proposed by is used:

$$\frac{\varepsilon - \varepsilon_{mf}}{1-\varepsilon} = \exp\left(\frac{z - z_i}{Z_0}\right) \tag{5}$$

Solid volume fraction has an approximately parabolic form and is considered as follows [53]:

$$\frac{\varepsilon_p}{\bar{\varepsilon}_p} = 1 - \frac{\beta'}{2} + \beta'\left(\frac{r}{R_b}\right)^2 \tag{6}$$

where the value of β' falls in the range of $1.3 \leqslant \beta' \leqslant 1.9$ and β' increases with increasing superficial gas velocity and decreasing riser diameter [53]. β' value is taken as 1.3 in the model calculations with which the best results are obtained [42].

The pressure drop through the bottom zone is equal to the weight of the solids in this region and is considered only in axial direction. In the upper zone, pressure drop due to the hydrostatic head of solids is considered in axial direction while pressure drop due to solids acceleration is also considered in axial and radial directions. Having determined the voidage and velocity profiles of solids, in the model acceleration component of pressure drop is calculated as follows:

$$\nabla P_{\text{acc}} = \frac{1}{2}\rho\nabla(v^2\varepsilon_p) \tag{7}$$

The solids friction and gas friction components of pressure drop are considered as boundary conditions in momentum equations for solid and gas phases, respectively in the model. The solids friction is defined as the frictional force between the solids and the wall, while the gas friction is the frictional force between the gas and the wall. Hydrodynamic model used in this study has been developed in our previous studies [39,40]. The conservation of mass and momentum equations and the constitutive relations used in the hydrodynamic model are given in Table 1. Hydrodynamic model takes into account the axial and radial distribution of voidage and velocity, for gas and solid phase, pressure drop for gas phase and solids volume fraction and particle size distribution for solid phase. In order to determine the validity of the hydrodynamic model, the model results are compared with test results using the same input variables in the tests as the simulation program input. Hydrodynamic model results

Table 1
The conservation of mass and momentum equations for each phase and the constitutive relations

Gas phase	Solid phase
Continuity equation	
$\frac{d(C_j\varepsilon_i)}{dt} = \sum_{\text{in}} \dot{n}_j\varepsilon_i - \sum_{\text{out}} \dot{n}_j\varepsilon_i + \dot{R}_{g,j} + \dot{J}_{g,j}$	$\frac{d(\rho_j\varepsilon_{p,i})}{dt} = \sum_{\text{in}} \dot{m}_j\varepsilon_{p,i} - \sum_{\text{out}} \dot{m}_j\varepsilon_{p,i} + \dot{R}_{s,j} + \dot{J}_{s,j}$
$(j = \text{O}_2, \text{CO}, \text{CO}_2, \text{NO}, \text{N}_2\text{O}, \text{N}_2, \text{HCN}, \text{CNO}, \text{NH}_3, \text{H}_2\text{O}, \text{SO}_2, \text{CH}_4)$	$(j = \text{Char, Limestone, Bed material})$
Momentum equation	
$\frac{\partial(Cu\varepsilon_i)}{\partial t} + \frac{\partial(Cu\varepsilon_i u)}{\partial r} = -\frac{\partial(P\varepsilon_i)}{\partial r} - \frac{\partial(\tau_{rr}\varepsilon_i)}{\partial r} - \frac{\partial(\tau_{rz}\varepsilon_i)}{\partial z} - \beta(u-v)$	$\frac{\partial(\rho v\varepsilon_{p,i})}{\partial t} + \frac{\partial(\rho v\varepsilon_{p,i} v)}{\partial r} = -\frac{\partial(\tau_{rr}\varepsilon_{p,i})}{\partial r} - \frac{\partial(\tau_{rz}\varepsilon_{p,i})}{\partial z} + \beta(u-v) - \frac{\partial(G(\varepsilon)\varepsilon_{p,i})}{\partial r}$
$\frac{\partial(Cu\varepsilon_i)}{\partial t} + \frac{\partial(Cu\varepsilon_i u)}{\partial z} = -\frac{\partial(P\varepsilon_i)}{\partial z} - \frac{\partial(\tau_{zz}\varepsilon_i)}{\partial z} - \frac{\partial(\tau_{zr}\varepsilon_i)}{\partial r} - \beta(u-v)$	$\frac{\partial(\rho v\varepsilon_{p,i})}{\partial t} + \frac{\partial(\rho v\varepsilon_{p,i} v)}{\partial z} = -\frac{\partial(\tau_{zz}\varepsilon_{p,i})}{\partial z} - \frac{\partial(\tau_{zr}\varepsilon_{p,i})}{\partial r} + \beta(u-v) - \frac{\partial(G(\varepsilon)\varepsilon_{p,i})}{\partial z} + \rho g\varepsilon_{p,i}$
$\tau_{rr} = 2\mu\frac{\partial u}{\partial r} - \frac{2}{3}\mu\left(\frac{\partial u}{\partial r} + \frac{\partial u}{\partial z}\right)$ *Ideal gas equation*	$\tau_{rr} = 2\mu\frac{\partial v}{\partial r} - \frac{2}{3}\mu\left(\frac{\partial v}{\partial r} + \frac{\partial v}{\partial z}\right)$ *Solids stress modulus*
$\tau_{zz} = 2\mu\frac{\partial u}{\partial z} - \frac{2}{3}\mu\left(\frac{\partial u}{\partial z} + \frac{\partial u}{\partial r}\right)$ $C = \frac{1}{R_u}\frac{P}{T}$	$\tau_{zz} = 2\mu\frac{\partial v}{\partial z} - \frac{2}{3}\mu\left(\frac{\partial v}{\partial z} + \frac{\partial v}{\partial r}\right)$ $G(\varepsilon) = \frac{\partial\tau}{\partial(1-\varepsilon)} = 10^{-8.76\cdot\varepsilon+5.43}$
$\tau_{rz} = \tau_{zr} = \mu\left(\frac{\partial u}{\partial z} + \frac{\partial u}{\partial r}\right)$	$\tau_{rz} = \tau_{zr} = \mu\left(\frac{\partial v}{\partial z} + \frac{\partial v}{\partial r}\right)$
Gas–solid friction coefficient [14]	$C_D = \frac{24}{Re_p}(1 + 0.15Re_p^{0.687})$ $Re_p < 1000$
$\beta = \frac{3}{4}C_D\frac{C\varepsilon_i(1-\varepsilon_i)}{\varepsilon_i^{2.65}}\frac{1}{d_p}\lvert u-v\rvert$	$C_D = 0.44$ $Re_p \geqslant 1000$

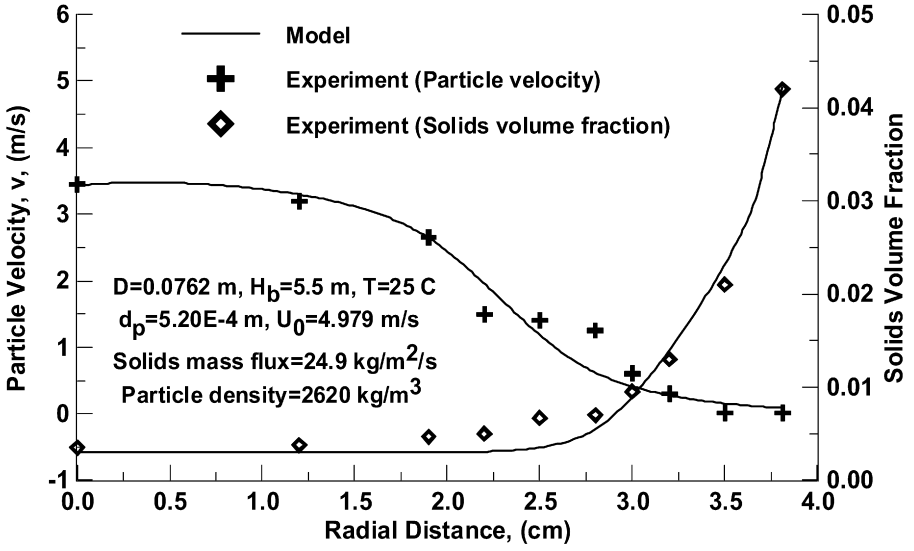

Fig. 2. Comparison of hydrodynamic model with Luo [54]'s experimental data.

are compared with experimental results obtained from various CFB test rigs at different size in the literature. The model compares with experimental results for void fraction, solids volume fraction, and particle velocity along the bed height and bed radius and different bed operational parameters prove the model hydrodynamic structure validation axially and radially. Additionally inward solids mass flux along the bed radius and pressure gradient along the bed height is validated. Fig. 2 shows the comparison of previous model's results with Luo [54]'s experimental data as an example of earlier model validation for the solids volume fraction and particle velocity values at mean particle diameter of 520 μm. The solids particles are entrained up the column, against gravity, by the upflowing gas flow. The radial profile is relatively flat in the core and solids volume fraction increases sharply toward the wall in the annulus with the highest solids volume fraction right at the wall. The coexistence of a dense annulus and dilute core can be easily recognized. Surrounding the core, there is an annular dense region near the wall where particle concentration is higher and most particles fall downwards. The non-uniform radial distribution of the lo-

cal particles axial velocity is a major flow character in risers. In the riser, the overall radial structure in terms of the particle velocity also shows a core-annulus style where the particles move faster in the core, slower in the annulus with the highest velocity at the centre. Normally, the local particle velocity decreases monotonically from the centre toward the wall as it is clearly seen in Fig. 2. A more detailed study on developed hydrodynamic model of the previous studies can be found in the literature [39,40].

2.2. Kinetic model

The char comprises mainly carbon, ash, nitrogen and sulphur. Above 750 °C, char oxidizes to gaseous products; CO, CO_2, SO_2 and NO_x. In all the current steady state or dynamic models in the literature, the assumption is made that coal is volatilized in the bottom zone; the resultants stay within that region and never enter the upper region [10,14,17]. As a result of the experimental studies carried out using various types of Turkish lignite, it is known that volatilization products enter the upper region in fluid beds working at slower rates than CFBs [55–57]. Experiments with CFBs give the same results. Therefore the transition of these products should be taken into consideration in modeling, depending on solid mixing. In the model, volatiles are entering the combustor with the fed coal particles. It is assumed that the volatiles are released in emulsion phase in the bottom zone of the CFB combustor at a rate proportional to the solid mixing rate. The degree of devolatilization and its rate increase with increasing temperature [58]. Volatile yield is estimated by the following empirical correlations in the model given by Gregory and Littlejohn [59],

$$V = VM - A - B \tag{8}$$

$$A = \exp(26.41 - 3.961 \cdot \ln T + 1.15 \cdot VM)/100 \tag{9}$$

$$B = 0.2 \cdot (VM - 0.109) \tag{10}$$

The composition of the products of devolatilization in weight fractions is estimated from the following correlations [60]:

$$\mathrm{CH_4} = 0.201 - 0.469 \cdot VM + 0.241 \cdot VM^2 \tag{11}$$

$$\mathrm{H_2} = 0.157 - 0.868 \cdot VM + 1.388 \cdot VM^2 \tag{12}$$

$$\mathrm{CO_2} = 0.135 - 0.900 \cdot VM + 1.906 \cdot VM^2 \tag{13}$$

$$\mathrm{CO} = 0.428 - 2.653 \cdot VM + 4.845 \cdot VM^2 \tag{14}$$

$$\mathrm{H_2O} = 0.409 - 2.389 \cdot VM + 4.554 \cdot VM^2 \tag{15}$$

$$\mathrm{Tar} = -0.325 + 7.279 \cdot VM - 12.880 \cdot VM^2 \tag{16}$$

The amount of volatile nitrogen and sulphur increases as a function of bed temperature and during devolatilization is expressed as [61],

$$\mathrm{N} = 0.001 \cdot T - 0.6 \ (\mathrm{kg/kg\ coal}) \tag{17}$$

$$\mathrm{S} = 0.001 \cdot T - 0.06 \ (\mathrm{kg/kg\ coal}) \tag{18}$$

The combustor model takes into account the devolatilization of coal, and subsequent combustion of volatiles followed by residual char. The rates of burning of CH_4, H_2 and CO are considered in the model as given in Table 2.

The char particles resulting from the devolatilization process consist of the remaining carbon fraction $(1 - X_c)$ and ash only. A char particle may take 1–10 s (depending upon the riser height) to pass through the bed riser once. However, as the particle is likely to make many trips around the CFB loop, the total residence time could be as much as 10 000 s, depending on the solid inventory, feed rate, coal size, etc. [33]. The total residence time of a char particle in the riser should exceed its burn out time. If that does not happen, the residual part of the char leaves the bed unburnt. Thus an adequate description of the burning of char particles in the CFB is important. In the model, the char combustion at each control volume is considered according to the reaction and its reaction rate which are given in Table 2. Combustion of coal is depending on oxygen presence in the bed. The mechanism factor, Φ is equal to 1.0 for CO_2 transport from the surface, and is equal to 2.0 for CO transport [51].

Understanding the mechanism of NO_x formation is needed to reduce NO_x in the combustor. However, the mechanism of NO_x formation is complex. NO_x formations in combustion processes result from a combination of a thermal generation process and fuel nitrogen oxidation. At very high temperatures, thermal generation of NO_x from the air nitrogen becomes very important, while at low temperatures found in a CFB combustor, the dominant source of NO_x is fuel nitrogen oxidation [23–25]. Typically, significant amounts of the fuel-nitrogen remain in the char after the devolatilization. The oxidation of this char-nitrogen gives an important contribution to the total nitrogen oxide emissions from the combustor. The mechanism of char-nitrogen oxidation to the products is very complex, and includes not only several homogeneous and heterogeneous reactions but also mass transfer effects inside the pore system of the char and in the boundary layer surrounding the particle [28]. In the present study, NO_x reactions and reaction rates using in the model are given in Table 2.

CFBs offer the possibility of removing the sulphur dioxide during combustion by adding limestone ($CaCO_3$) directly to the combustion chamber. Using such limestone directly with a fuel inserted to the combustion chamber leads to highly efficient desulphurization. During the combustion of coal, the sulphur in it is oxidized to the pollutant, SO_2. Limestone ($CaCO_3$) of the bed materials calcine to CaO which reacts with SO_2 producing $CaSO_4$. Thus instead of leaving the combustor as a gaseous pollutant sulphur is discharged as a solid residue [10]. In CFB combustor the SO_2 generation and retention processes take place simultaneously in the bed [64]. Table 2 shows the all reactions and reaction rates used in the model.

The properties and size distribution of particles have significant influence on the hydrodynamics and combustion behavior in the CFB furnace [16]. The model also considers the particle size distribution due to fuel particle fragmentation, char combustion and particle attrition. In CFBs, fragmentation of coal particles in a fluidized bed occur within a few seconds after injection of the particles into the bed due to build-up of thermal and devolatilization-induced stresses [65,66]. It may be assumed that primary fragmentation occurs primarily in the zones

Table 2
The reactions and reaction rates used in the model

Reaction	Reaction rate	
$C + \frac{1}{\Phi}O_2 \rightarrow (2 - \frac{2}{\Phi})CO + (\frac{2}{\Phi} - 1)CO_2$	$R_c = \pi d_c^2 k_c C_{O_2}$ ($\frac{mol}{s}$)	$k_{cr} = 8710 \cdot \exp\left(\frac{-1.4947 \cdot 10^8}{R_u \cdot T}\right)$ ($\frac{kg}{m^2\,s\,kPa}$) [73]
	$k_c = \frac{R_u T / M_c}{1/k_{cr} + 1/k_{cd}}$ ($\frac{kg}{s}$)	$k_{cd} = \frac{12 \cdot Sh \cdot \Phi \cdot D_g}{d_p \cdot R_g \cdot T}$ ($\frac{kg}{m^2\,s\,kPa}$)
	$Sh = \frac{k_g d_p}{D_g} = 2\varepsilon + 0.69\left(\frac{Re_p}{\varepsilon}\right)^{1/2} Sc^{1/3}$ [15,17]	
$CO + \frac{1}{2}O_2 \rightarrow CO_2$	$R_{CO} = 3 \cdot 10^{10} \exp\left(\frac{-6.699 \cdot 10^7}{R_u T}\right) y_{CO} y_{H_2O}^{0.5} \frac{17.5 \cdot y_{O_2}}{1 + 24 \cdot y_{O_2}} \left(\frac{P}{R_u T}\right)^{1.8}$ ($\frac{mol}{cm^3\,s}$) [62]	
$CO_2 + C \rightarrow 2CO$	$R_{CO_2C} = N\pi d_p^2 k C_{CO_2}$ ($\frac{mol}{s}$) [10,14,51]	$k = 4.1 \cdot 10^6 \exp\left(\frac{-29787}{T}\right)$
$CH_4 + \frac{3}{2}O_2 \rightarrow CO + H_2O$	$R_{CH_4} = k C_{O_2}^{0.8} C_{CH_4}^{0.7}$ ($\frac{mol}{m^3\,s}$) [63]	$k = 1.585 \cdot 10^{10} \exp\left(\frac{-24157}{T}\right)$
$2H_2 + O_2 \rightarrow 2H_2O$	$R_{H_2} = k C_{O_2} C_{H_2}^{1.5}$ ($\frac{mol}{m^3\,s}$) [63]	$k = 1.63 \cdot 10^9 T^{1.5} \exp\left(\frac{-3420}{T}\right)$
$HCN + \frac{1}{2}O_2 \rightarrow CNO$	$R_{HCN} = k C_{O_2} C_{HCN}$ ($\frac{mol}{m^3\,s}$) [63]	$k = 2.14 \cdot 10^5 \exp\left(\frac{-10000}{T}\right)$
$CNO + \frac{1}{2}O_2 \rightarrow NO + CO$	$R_{CNO\text{–}O_2} = k C_{O_2} C_{HCN}\left(\frac{k_1}{k_1 + k_2 C_{NO}}\right)$ ($\frac{mol}{m^3\,s}$) [63]	$\frac{k_2}{k_1} = 1.02 \cdot 10^9 \exp\left(\frac{-25460}{T}\right)$
$CNO + NO \rightarrow N_2O + CO$	$R_{CNO\text{–}NO} = k C_{O_2} C_{HCN}\left(\frac{k_2 C_{NO}}{k_1 + k_2 C_{NO}}\right)$ ($\frac{mol}{m^3\,s}$) [63]	$k = 2.14 \cdot 10^5 \exp\left(\frac{-10000}{T}\right)$
$N_2O + C \rightarrow N_2 + CO$	$R_{N_2OC} = kN\pi d_c^2 C_{N_2O}$ ($\frac{mol}{s}$) [29]	$k = 2.9 \cdot 10^9 \exp\left(\frac{-16983}{T}\right)$
$N_2O + CO \rightarrow N_2 + CO_2$	$R_{N_2O\text{–}CO} = k C_{N_2O} C_{CO}$ ($\frac{mol}{cm^3\,s}$) [29]	$k = 5.01 \cdot 10^{13} \exp\left(\frac{-4.40 \cdot 10^4}{R_u T}\right)$
$N_2O + \frac{1}{2}O_2 \rightarrow N_2 + O_2$	$R_{N_2O\text{–}O_2} = k C_{N_2O} C_{O_2}$ ($\frac{mol}{cm^3\,s}$) [29]	$k = 1.00 \cdot 10^{14} \exp\left(\frac{-2.80 \cdot 10^4}{R_u T}\right)$
$NO + C \rightarrow \frac{1}{2}N_2 + CO$	$R_{NOC} = kN\pi d_c^2 C_{NO}$ ($\frac{mol}{s}$) [63]	$k = 5.85 \cdot 10^7 \exp\left(\frac{-12000}{T}\right)$
$NO + \frac{1}{2}C \rightarrow \frac{1}{2}N_2 + \frac{1}{2}CO_2$	$R_{2NOC} = kN\pi d_c^2 C_{NO}$ ($\frac{mol}{s}$) [28]	$k = 1.3 \cdot 10^5 \exp\left(\frac{-17111}{T}\right)$
$NO + CO \rightarrow \frac{1}{2}N_2 + CO_2$	$R_{NOCO} = KT \frac{(k_1 C_{NO}(k_2 C_{CO} + k_3))}{(k_1 C_{NO} + k_2 C_{CO} + k_3)}$ ($\frac{mol}{m^3\,s}$) [63]	$KT = 1.952 \cdot 10^{10} \exp\left(\frac{-19000}{T}\right)$ $k_1 = 0.1826,\ k_2 = 0.00786$ $k_3 = 0.002531$
$NH_3 + \frac{5}{4}O_2 \rightarrow NO + \frac{3}{2}H_2O$	$R_{NH_3NO} = k C_{NH_3} C_{O_2}$ ($\frac{mol}{m^3\,s}$) [63]	$k = 2.73 \cdot 10^{14} \exp\left(\frac{-38160}{T}\right)$
$NH_3 + \frac{3}{4}O_2 \rightarrow \frac{1}{2}N_2 + \frac{3}{2}H_2O$	$R_{NH_3N_2} = \frac{k C_{NH_3} C_{O_2}}{C_{O_2} + k'}$ ($\frac{mol}{m^3\,s}$) [63]	$k = 3.38 \cdot 10^7 \exp\left(\frac{-10000}{T}\right),\ k' = 0.054$
$NO + NH_3 + \frac{1}{2}O_2 \rightarrow N_2 + \frac{3}{2}H_2O$	$R_{NONH_3} = k\sqrt{C_{O_2}}\sqrt{C_{NH_3}}\sqrt{C_{NO}}$ ($\frac{mol}{m^3\,s}$) [63]	$k = 1.1 \cdot 10^{12} \exp\left(\frac{-27680}{T}\right)$
$CaO + SO_2 + \frac{1}{2}O_2 \rightarrow CaSO_4$	$k_L = \frac{\pi}{6} d_s^3 k_{vL} C_{SO_2}$ ($\frac{1}{s}$) [15,64,74]	$k_{vL} = 490 \exp\left(\frac{-17500}{R_g T}\right) S_g \lambda_s$ ($\frac{kg}{m^2\,s}$) [34] $S_g = -384 T_g + 5.6 \times 10^4, \quad T_g \geqslant 1253$ K $S_g = 35.9 T_g - 3.67 \times 10^4, \quad T_g < 1253$ K

close to the feed ports. The following expression is used as the fragmentation of particles in the model [66]:

$$P(d_{p,\text{new}}) = k_f^{0.33} P(d_{p,\text{old}}) \quad \text{with } d_{p,\text{new}} = d_{p,\text{old}} k_f^{0.33} \tag{19}$$

where $P(d)$ is the particle size distribution function; $d_{p,\text{new}}$ and $d_{p,\text{old}}$ are the particle diameters after fragmentation and before fragmentation, respectively, k_f the fragmentation coefficient. Bellgardt et al. [66] suggest that the fragmentation constant k_f falls between 1 and 2 for a bubbling fluidized bed. Because of the higher superficial gas velocity, fragmentation in a CFB may have more pronounced effects on chemical reaction than in a bubbling fluidized bed.

The bed material in the combustor consists of coal, inert particles and limestone. Particles in the model are divided into 10 size groups in the model. Particles in the bottom zone include particles coming from the solid feed and recirculated particles from the separator. The proper size and distribution of solid inventory influences the heat absorption and indirectly the combustion and pollutant generation. Mean particle diameter of different-sized particles is considered as follows:

$$d_p = 1 \Big/ \sum_{i=1}^{n} \frac{x_i}{d_{pi}} \tag{20}$$

While moving in the combustor, the char particle burns and undergoes attrition. In the fluidized beds, particle attrition takes place by surface abrasion, i.e. particles of a much smaller break away from the original particle. The upper limit size of the fines

produced is in the range 50–100 μm [67,68]. The particle attrition rate differs significantly between the bottom zone and the upper zone due to different hydrodynamic properties. In the model, the attrition rate for the bottom zone is calculated as follows [68]:

$$R_a = k_a(U_0 - U_{mf})\frac{W_b}{d_p} \tag{21}$$

For the upper zone, attrition rate is defined in terms of gas and solid velocities;

$$R_a = k_a(u - v)\frac{W_b}{d_p} \tag{22}$$

where k_a is the attrition constant and is obtained varying in the range $2–7 \times 10^{-7}$ with a superficial gas velocity of 4–6 $\mathrm{m\,s^{-1}}$ and a circulating solids mass flux from 100 to 200 $\mathrm{kg\,m^{-2}\,s^{-1}}$ [16]. In the model, the attrition constant value is taken as 2×10^{-7} for the coal particles in the model calculations in both bottom zone and upper zone [55,56]. After the combustion of char, ash is the residual product which takes no part in the combustion reaction. It can be assumed that only the ash layer is worn out as the particle undergoes reactions following a dual shrinking-core model. It is observed that a coarse ash particle drained from the bottom of a CFB boiler has an unburnt carbon core wrapped by a spent ash layer. This indicates that only the ash layer of such particles is gradually worn out by attrition in the combustor [16]. In the model, the attrition constant value is taken as 1.7×10^{-7} for the attrition constant of the coal ash particles [55,56]. In the model, Eqs. (21) and (22) are used to determine the attrition rate of limestone particles for the bottom zone and the upper zone respectively.

Weight fraction of particles after attrition is considered as follows:

$$x_a = \frac{k_a(u - v)}{d_{pi}} \tag{23}$$

Coal particles' behavior during the gas–solid reaction is assumed to be described in terms of shrinking core with attiring shell, i.e. the dual shrinking-core model. The rate at which particles of size r_i shrink as follows [17]:

$$r(r_i) = -\frac{dr_i}{dr} = \frac{12C_{O_2}}{\rho X_{k,i}(1/k_{c,i} + d_{p,i}/Sh_i D_g)} \tag{24}$$

2.3. Heat transfer

The overall heat transfer coefficient from bed to wall at the bottom section is given by Basu and Nag [69] as

$$h = 40(\rho_b)^{1/2} \tag{25}$$

where ρ_b is the local bed density; $\rho_b = \rho(1 - \varepsilon) + C\varepsilon$. In the upper zone, based on the special hydrodynamics of the CFB combustor, the cluster renewal model of the bed to the wall heat transfer process has been described in the literature [10,63]. The dilute phase is comprised of a continuous upflowing gas phase with thinly dispersed solids and a relatively denser phase moving downward along the heat transfer surfaces. The cluster renewal model which is used in the simulation is shown in Fig. 3.

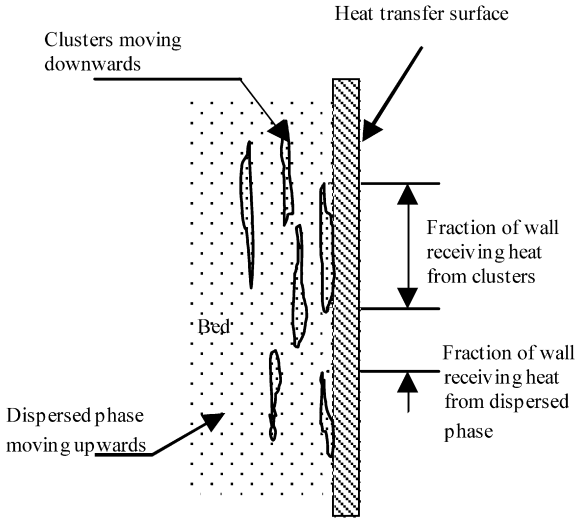

Fig. 3. Cluster renewal model.

If ε_c is the average fraction of the wall area covered by the clusters, the time-averaged total heat transfer coefficient, h_t, may be written as the sum of the convective and radiative heat transfer coefficients [68–70]:

$$h_t = \varepsilon_c h_c + (1 - \varepsilon_c)h_d + \varepsilon_c h_{rc} + (1 - \varepsilon_c)h_{rd} \tag{26}$$

The energy equation for each control volume is considered as follows:

$$\begin{aligned} &C\varepsilon_i c_v\frac{\partial T}{\partial t} - uC\varepsilon_i c_v\frac{\partial T}{\partial r} - uC\varepsilon_i c_v\frac{\partial T}{\partial z} + \rho\varepsilon_{p,i}c_p\frac{\partial T_p}{\partial t} \\ &\quad - u\rho\varepsilon_{p,i}c_p\frac{\partial T_p}{\partial r} - u\rho\varepsilon_{p,i}c_p\frac{\partial T_p}{\partial z} \\ &= R''' + \mu\varepsilon_i\left\{2\left[\left(\frac{\partial u}{\partial r}\right)^2 + \left(\frac{\partial u}{\partial z}\right)^2\right] + \frac{1}{3}\left(\frac{\partial u}{\partial r} + \frac{\partial u}{\partial z}\right)^2\right\} \\ &\quad + \mu\varepsilon_i\left\{2\left[\left(\frac{\partial v}{\partial r}\right)^2 + \left(\frac{\partial v}{\partial z}\right)^2\right] + \frac{1}{3}\left(\frac{\partial v}{\partial r} + \frac{\partial v}{\partial z}\right)^2\right\} \end{aligned} \tag{27}$$

3. Numerical solution

The model should be flexible enough in order to be used in different applications of CFBs. The computer code should be modular to allow users to update component modules easily as new findings become available. The set of differential equations governing mass, momentum and energy for the gas and solid phases are solved using an IBM-PC-Pentium4 (CPU speed is 2800 MHz) with a computer code developed by the authors in FORTRAN language where the time step is 10^{-6} seconds. In these equations, the dependent variables are the vertical and the horizontal components of the void fraction, the solid volume fraction, the gas pressure, the gas concentration, the vertical and the horizontal velocity and temperature components of the gas and solids. The Gauss–Seidel iteration which contains successful relaxation method and combined Relaxation Newton–Raphson methods are used for solution procedure. The backward-difference method is used the discretization of the governing equations (Table 1 and Eq. (15)).

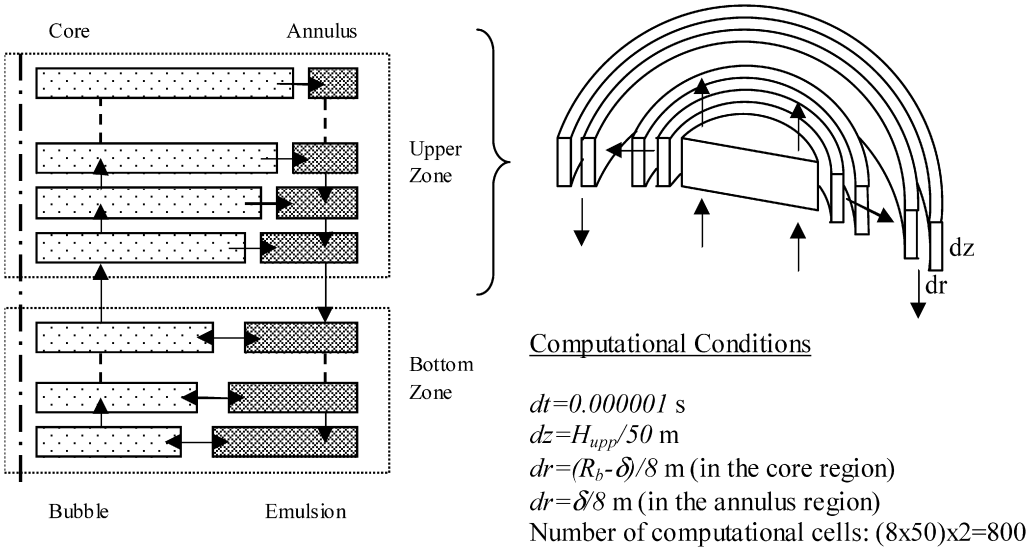

Fig. 4. Particle flux structure, control volumes in the upper zone and computational conditions in the CFB riser.

The simulation geometry of the control volumes is shown in Fig. 4. The model allows dividing the calculation domain into $m \times n$ control volumes, in the radial and the axial directions and in the core and the annulus regions respectively. In this study the calculation domain is divided into 8×50 control volumes in the radial and the axial directions and in the core and the annulus regions respectively. The control volumes are chosen to be uniform in the axial direction, whereas non-uniform control volumes are used in radial direction where the smaller control volumes exist in the annulus region. This difference is increasing while bed height increases, because of the thickness of annulus is very small when compared to the core region and decreases with bed height. With the cylindrical system of coordinates, a symmetry boundary condition is assumed at the column axis.

At the walls, a partial slip condition is assumed for the solid and the gas phases. In the model, the frictional force between the gas and the wall is considered as follows:

$$\left\{ \begin{matrix} \text{Gas} \\ \text{friction} \end{matrix} \right\} = \frac{2 f_g \varepsilon C u^2}{dz} \tag{28}$$

where f_g is wall friction factor of gas phase. Modified Hagen–Poiseuille expression is used for wall friction factor of gas phase in the model and is as follows [71]:

$$f_g = \begin{cases} 16/Re_g, & Re_g \leqslant 2100 \\ 0.0791/Re_g^{0.25}, & 2100 < Re_g \leqslant 100\,000 \end{cases} \tag{29}$$

The frictional force between the solids and the wall is considered as follows:

$$\left\{ \begin{matrix} \text{Solids} \\ \text{friction} \end{matrix} \right\} = \frac{2 f_s \varepsilon_p \rho v^2}{dz} \tag{30}$$

where f_s is wall friction factor of solid phase. Konno's correlation is used for wall friction factor of solid phase in the model as follows [71]:

$$f_s = 0.0025 \cdot v^{-1} \tag{31}$$

In the model, it is assumed that the particles move upward in axially and move from core to the annulus region in radially. In general, when a rigid particle strikes the wall it rebounds either fully or partially. In the annulus region, it is assumed that the particle has a zero normal velocity. Because of assuming a partial slip condition for the solid phase, for the tangential direction along the wall surface the particle velocity is determined according to the results of momentum equation. Particles are discretized into 10 groups totally. The particle size distribution depends on fragmentation, combustion and attrition in the bed. The particle size distribution for small-scale unit is shown in Fig. 5. As mentioned above the Sauter mean diameter is adopted as average particle size (Eq. (20)).

Inputs for the model are combustor dimensions and construction specifications (insulation thickness and materials, etc.), primary and secondary air flow rates; coal feed rate and particle size distribution, coal properties, Ca/S ratio, limestone particle size distribution, inlet air pressure and temperature, ambient temperature and the superficial velocity. A continuity condition is used for the gas phase at the top of the cyclone. The cyclone is considered to have 98% collection efficiency.

4. Model validation

To validate the combustor model presented in this study, simulation results are compared with two different size CFB combustor, which use different kinds of Turkish Lignite, the 50 kW pilot CFB combustor using Tuncbilek lignite at the Gazi University Heat Power Laboratory and an industrial-scale 160 MW CFB combustor using Can lignite at Can Power Plant, obtained during the commissioning period [41,42].

Firstly, simulation results are compared with test results obtained from 50 kW laboratory scale test unit of 12.5 cm i.d., 180 cm tall main column (riser). The riser of 0.31 m outer diameter was made of stainless steel and was insulated from inside with insulation material (fire bricks) down to the diameter of 0.125 m. The combustion air is supplied through the distributor

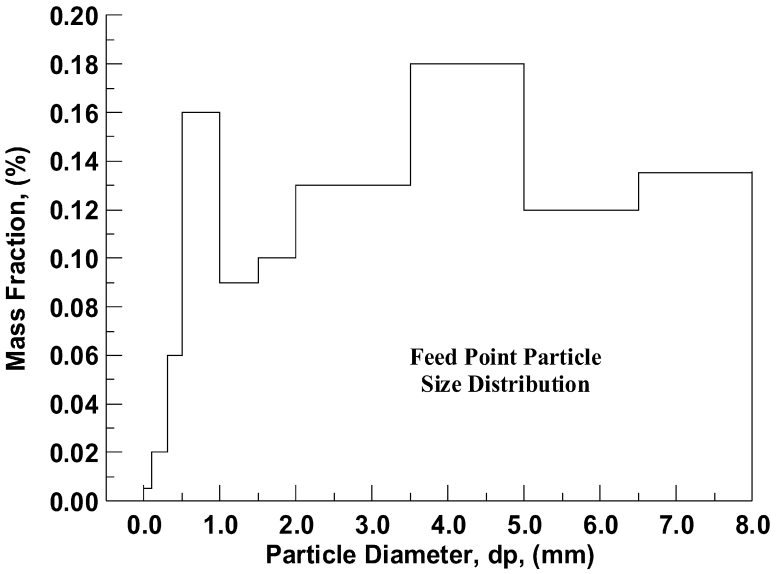

Fig. 5. Particle size distribution.

(primary air) by a blower of capacity with 1000 m^3/h (7.5 hp), and the secondary air inlets are located at 0.4 m above the distributor, two high efficiency cyclones in series, a re-circulation bed, fuel feeding and ash discharging systems and a flue gas analysis system [41]. A more detailed description of the experimental apparatus is given elsewhere [72]. Silica sand and ash were used as bed materials. The weighted average particle sizes in the experimental setup are determined to be 0.56 mm for sand particles.

In the experiments, in order to measure the gas concentrations along the bed height, multi channel gas sampling system was used. The combustor column is equipped with gas concentration measurement probes located at the combustor wall radially and at the height 0.2 m from the distributor plate and at 7 other regularly set heights 0.2 m distanced from each other axially to obtain the differential gas concentration profiles [41]. The analysis of the flue gas is carried out on the gas stream exiting from the secondary cyclone. After the gas is passed through a filtering system, O_2, CO, CO_2, NO_x and SO_2 concentrations are measured; O_2 is analyzed by a paramagnetic analyzer (sensitivity $\pm 1\%$), CO and CO_2 by NDIR (nondispersive infrared) analyzer (sensitivity $\pm 1\%$), SO_2 by NDUV (nondispersive ultraviolet) analyzer (sensitivity ± 2 ppm) and NO_x by chemiluminescence analyzer (sensitivity ± 1 ppm). The pressure drops in the distributor and in the bed are measured with manometers. The considered parameters and computation conditions are given in Table 3, including data from Topal [41] that are introduced to validate the simulation. The design fuel for the bed is low grade coal (Tuncbilek Lignite) and the compositions of coal used in experimental data are given in Table 4. The model predictions and experimental results are shown in Figs. 6–10.

Fig. 6 shows the measured and predicted oxygen and carbon dioxide mole ratios and sulphur dioxide emissions response in flue gases. The presented model considers the axial and radial distribution of voidage, velocity; particle size distribution, pressure drop; gas emissions and temperature for gas and solid phase for the bottom zone and the upper zone in detail and the simulated results are in good agreement with experimental ones. Since CFB under consideration is a small-scale CFB combustor, combustor reaches its steady-state conditions in a short time (in less than a few seconds) and, a significant deviation in the measured and predicted values has not been observed as the time interval increases.

To test and validate the model presented in this paper, also the molar ratio of oxygen, carbon monoxide, sulphur dioxide and NO_x emissions are compared using the same input variables in the tests as the simulation program input. Detailed listing of the model input variables are given in Table 5. The

Table 3
Operating parameters of the experimental data referred to in this study

Operating parameters	Pilot scale combustor [41]	Industrial scale combustor [42]
Coal feed rate (range)	6–7.7 kg h^{-1}	110–120 tons h^{-1}
Operation velocity (range)	3.60–9.23 m s^{-1}	4–6 m s^{-1}
Bed temperature	860–900 °C	850–900 °C
Primary/secondary air ratio	2/3	2/3
Bed area	0.0122 m^2	57.38 m^2
Size of coal feed (range)	0.03–0.9 mm	0.1–9.0 mm
Mean size of sorbent feed	0.071 mm	0.1–0.15 mm

Table 4
Coal properties

	Tuncbilek lignite	Can lignite
Carbon (wt%, dry)	59.29	66.10
Hydrogen (wt%, dry)	4.61	5.50
Nitrogen (wt%, dry)	2.10	2.25
Sulphur (wt%, dry)	1.81	8.40
Vol. mat. (wt%, dry)	24.30	25.50
Ash (wt%, dry)	20.60	30.40
Moisture (%)	20.80	21.40
Hu (kJ kg^{-1})	22083.15	11704.00

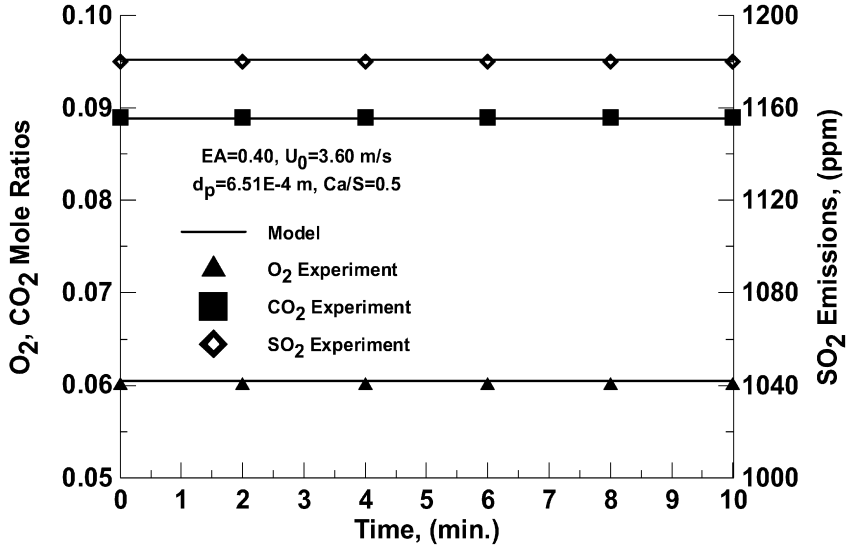

Fig. 6. Comparison of transient flue gas O_2 and CO_2 mole ratios, and SO_2 emissions with Topal [41]'s experimental data.

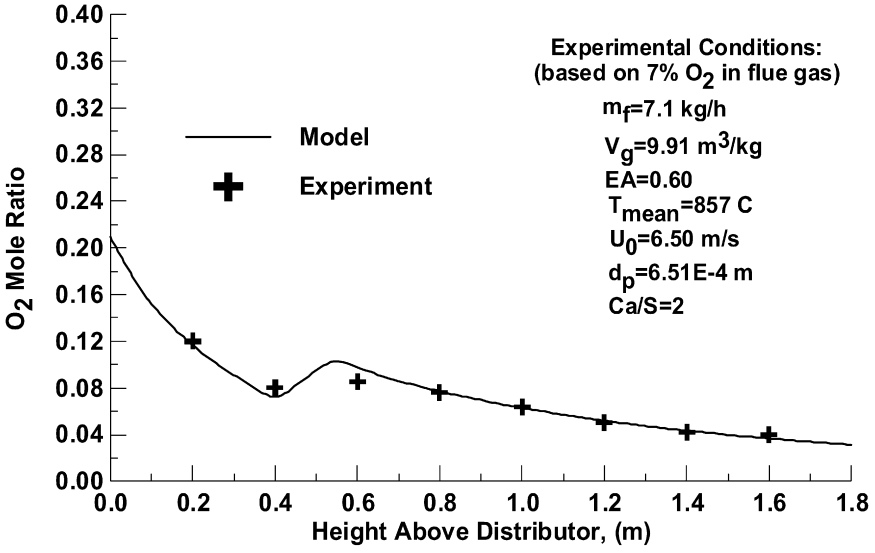

Fig. 7. Comparison of model O_2 mole ratio with Topal [41]'s experimental data. (The uncertainty of m_f is 0.18%, V_g is 0.10% and O_2 is 0.13%.)

measurements used in the comparison are derived from combustor wall. It must be noted that the gas concentrations in a CFB combustor depend on the radial position but since the data available for validation is obtained from the annulus region; the model considers gas concentrations for annulus region only. The measurements are based on O_2 concentration percentage in flue gas. To find the uncertainty in experimental measurements, standard deviation is calculated and it serves as a measure of uncertainty. For all measurements in the model validation, 0.60 value of excess air is used which has an uncertainty of 0.02%. The uncertainties of the other variables are given in Figs. 7–10.

In the present study, it is assumed that the volatiles are released in solid-laden emulsion phase in the bottom zone. The main consumption of oxygen in the bottom zone is due to the combustion of these volatiles. The char particles resulting from the devolatilization process consist of the remaining carbon fraction and ash only. These particles are then burned to produce a mixture of CO and CO_2. The combustion of coal particles and oxidation reaction of CO is the other O_2 consumption process in the combustor. In the bottom zone a significant change in the oxygen mole ratio is found, while in the upper region there is a gradual decrease in the oxygen mole ratio. Mole ratio of oxygen along the bed height is reasonably predicted by the model as shown in Fig. 7.

During staged combustion, under the secondary air injection because of not adequate oxygen presence due to the combustion of volatiles in the emulsion phase at the bottom zone, char combustion essentially leads to CO formation and carbon monoxide concentration is very high (Fig. 8). Oxygen in the annulus region increases while carbon monoxide emission sharply decreases due to secondary air supply at the 0.4 m. bed height above the distributor plate as shown in Figs. 7, 8. In addition to increment of oxygen mole ratio, sharp decrement in CO emis-

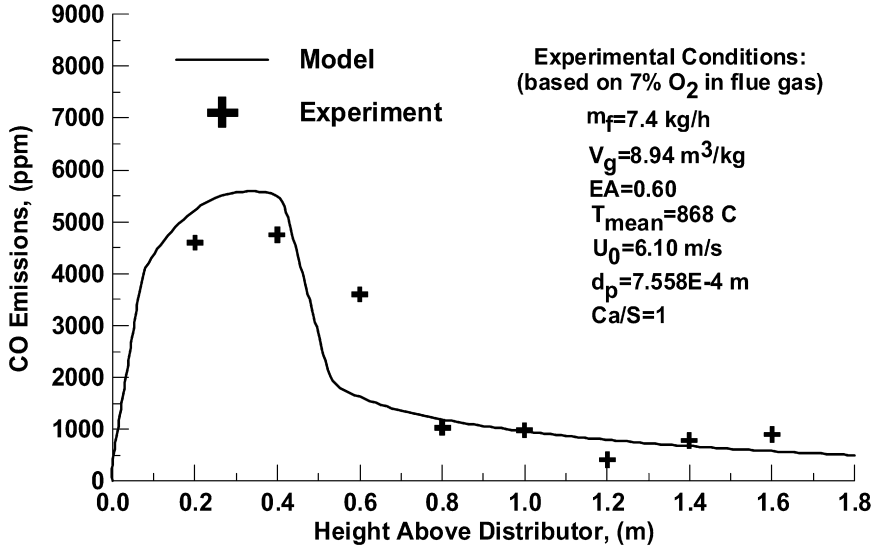

Fig. 8. Comparison of model CO emissions with Topal [41]'s experimental data. (The uncertainty of m_f is 0.2%, V_g is 0.08% and CO is 0.0007%.)

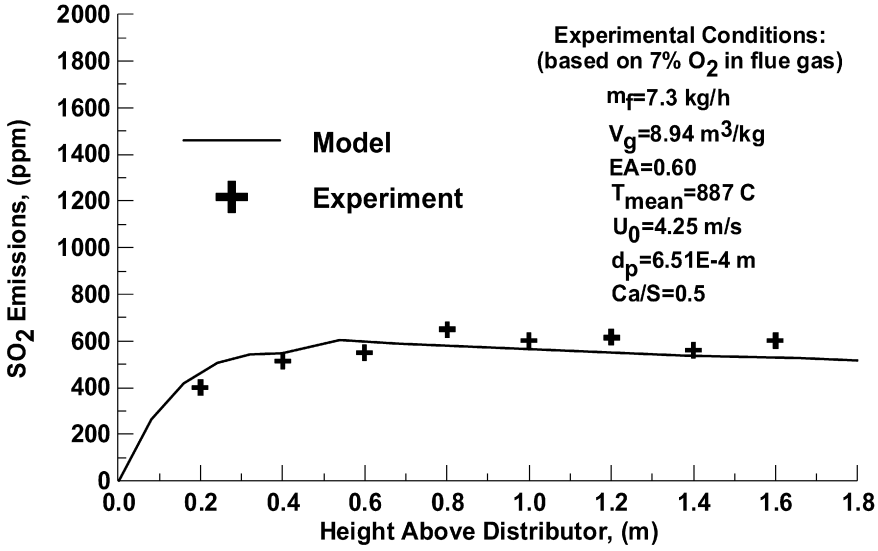

Fig. 9. Comparison of model SO_2 emissions with Topal [41]'s experimental data. (The uncertainty of m_f is 0.22%, V_g is 0.08% and SO_2 is 2 ppm.)

sions after the secondary air point is caused by the mechanism factor, depending on the bed temperature and coal particle diameter. However, discrepancies between the model results and experimental data are observed in Fig. 8. Because of hydrodynamic behavior of CFB combustor, fast fluidization in the bottom zone does not allow all carbon monoxide to be reduced to CO_2. So it leads to a discrepancy between the model results and experimental data.

As it is seen from the Fig. 9, SO_2 emissions along the combustor height are reasonably predicted by the model. An increase in SO_2 emissions is observed in the bottom zone due to the assumption that the great amount of the volatile matters is released at the feed point in the combustor. By getting better coal combustion with the secondary air feed (at the 0.4 m height above the distributor plate) it increases a certain amount of the fixed sulphur in its structure between the heights of 0.4 m and 0.6 m above the distributor plate. Above 0.6 m, adequate presence of oxygen due to secondary air feed increases the sulphur retention with limestone and simulation results show good agreement with experimental data as expected.

The increase of NO_x emissions at the bottom zone which is observed in Fig. 10 also indicates the release and combustion of volatiles and the combustion of char and could be influencing factors for the production of NO_x emissions. Nonexistence of a peak of NO_x in the bottom zone is caused by the fact that the experiments are carried out in a small-scale CFB and the values are measured at high superficial velocities such as 6.5 $m\,s^{-1}$. Secondary air feed leads to a better coal combustion and increases a certain amount of fixed nitrogen in coal between the heights of 0.4 m and 0.6 m above the distributor plate. The reduction of NO_x emissions is proportional to the presence of char particles and CO concentration in the control volume. High char particle concentration of annulus region leads to reducing NO_x emissions to an acceptable level. Staged combustion

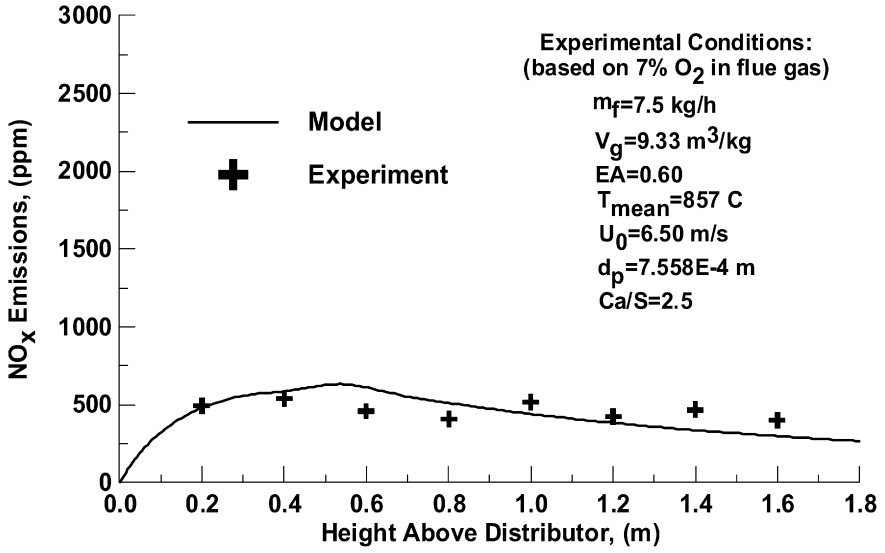

Fig. 10. Comparison of model NO_x emissions with Topal [41]'s experimental data. (The uncertainty of m_f is 0.1%, V_g is 0.22% and NO_x is 1 ppm.)

Table 5
Model input variables

Comparison element	D (m)	H_b (m)	H_{bot} (m)	Inlet pressure (atm.)	Excess air	Primary air/ secondary air	Superficial velocity ($m\,s^{-1}$)	Coal feed rate ($kg\,h^{-1}$)	Mean coal particle size (μm)	Mean bed temperature (°C)	Ca/S	Mean sorbent particle size (μm)
O_2	0.125	1.8	0.4	1.12	0.60	2/3	6.50	7.1	651	855	2.0	71
CO	0.125	1.8	0.4	1.12	0.60	2/3	6.10	7.4	755.8	866	1.0	71
SO_2	0.125	1.8	0.4	1.12	0.60	2/3	4.25	7.3	651	890	0.5	71
NO_x	0.125	1.8	0.4	1.12	0.60	2/3	6.50	7.5	755.8	851	2.5	71

Table 6
Comparison of simulation results with 2 × 160 MW Can Power Plant test results [42]

Time (min)	Coal feed ($tons\,h^{-1}$)	T (°C)		Err. (%)	NO_x ($mg\,m^{-3}$)		Err. (%)	SO_2 ($mg\,m^{-3}$)		Err. (%)
		Model	Data		Model	Data		Model	Data	
30	119.1	798.50	807.1	1.06	97.90	97.1	0.82	1290.55	1290.9	0.02
60	119	798.79	809.1	1.27	96.90	95.9	1.03	1274.08	1272.4	0.13
90	116.9	800.36	812.4	1.48	97.56	98.7	1.14	1183.50	1184.9	0.11
120	116.3	798.59	814.9	2.00	92.52	92.7	0.18	1235.86	1235.5	0.02
150	116	798.40	812.3	1.71	102.03	102.5	0.45	1185.11	1184.9	0.01
180	118.4	798.26	805.5	0.89	98.95	98.7	0.29	1205.80	1204	0.14
210	113.8	804.01	809.3	0.65	99.06	98.2	0.87	1240.32	1240.2	0.009

remains an attractive method for reducing NO_x emissions in various combustion systems. It is clearly seen from the Fig. 10 both experimental data and model simulation results have low and acceptable levels of gaseous emissions.

Simulation results are also compared with the data obtained from 2 × 160 MW Can Power Plant CFB combustors during the commissioning period, each with a 7 m × 14 m square cross-section and 37 m height [42]. The combustor has a square cross-section, but the lower section has less cross-sectional area than the upper section. The technical parameters of the CFB combustor are steam capacity of 485 $t\,h^{-1}$, superheated steam temperature and pressure of 543 °C and 17.5 MPa, respectively. The secondary air ports are located at 5 m from the distributor. The operating parameters of data used for the comparison of CFB model is shown in Table 3. The design fuel for the bed is low grade coal (Can Lignite) and the compositions of coal used in test data are given in Table 4. Temperature, sulphur dioxide and NO_x emissions response in flue gases simulation and test results at the riser exit were compared at different coal feed rates and the results are presented in Table 6. It is seen that the simulation results are in good agreement with industrial-scale CFB combustor data as well. Simulation results are in good agreement with both industrial and small-scale CFB combustors which is an indication that the model is flexible enough to be used in different CFB applications and simulates under a wide range of operating conditions.

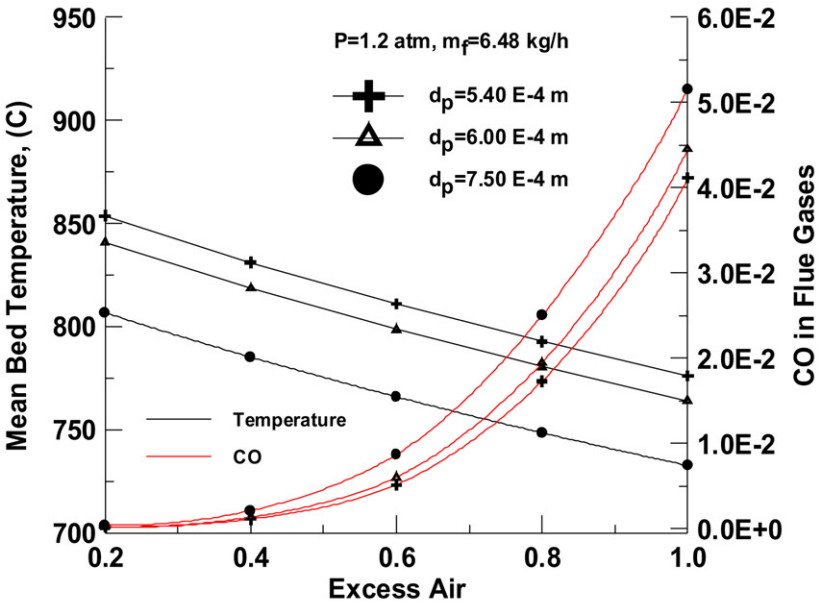

(a)

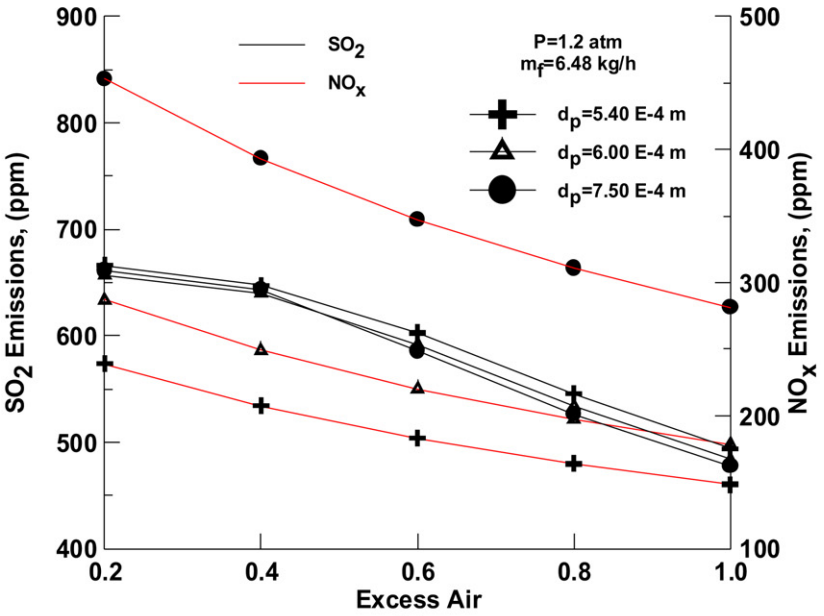

(b)

Fig. 11. Effect of excess air ratio on mean bed temperature and the overall CO, NO_x and SO_2 emissions from the combustor.

5. Sensitivity analysis

Sensitivity analysis has been performed to show how different model input values and assumptions affect the modeling results. In the present study, model input values of coal particle diameters, excess air ratios and bed operational velocities have been considered for sensitivity analysis. The modeling results under consideration in this study are mean bed temperature and emissions of CO, NO_x and SO_2.

Fig. 11 shows the effects of excess air and coal particle diameter on mean bed temperature and emissions of CO, NO_x and SO_2 in modeling results. Fig. 11 plots the predicted model results for three particle diameters (540, 600 and 750 μm) and for five excess air ratios (of about 20, 40, 60, 80 and 100%). For this assumption inlet bed pressure is 1.2 atm and coal feed rate is 6.48 kg h^{-1}.

As the excess air value increases, the mean bed temperature decreases due to higher heat losses with increasing flue gas flow rates to the ambient. This causes the reaction rate of char combustion to decrease, which leads to higher CO emission. Decreasing bed temperature generates a decrease of the CO oxidation rate constant. As it is seen from the Fig. 11(a), CO emissions increase when excess air increases. This phenomenon is also observed in the studies of Ducarne et al. [63].

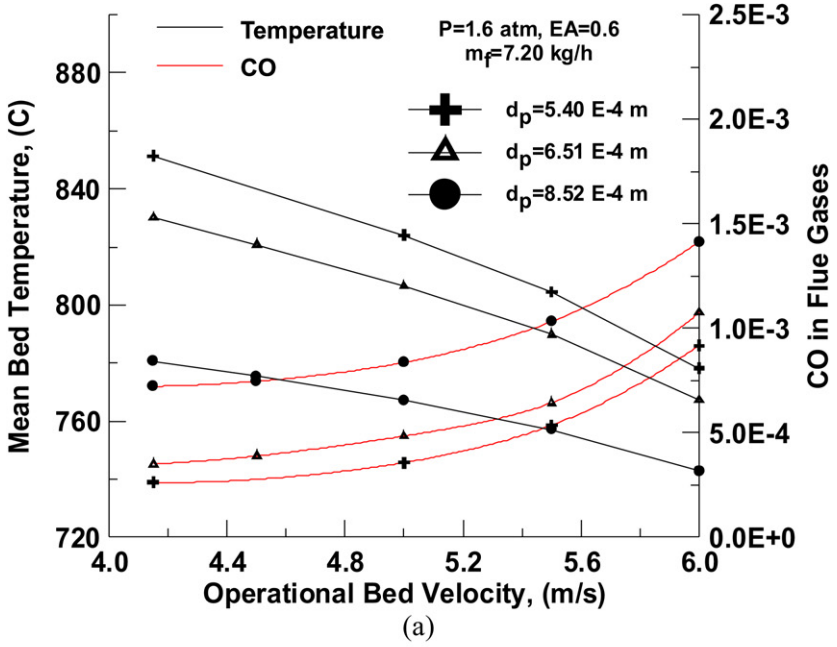

Fig. 12. Effect of operational bed velocity on mean bed temperature and the overall CO, NO_x and SO_2 emissions from the combustor.

Increasing excess air results in lower levels of NO_x formation which is generated due to combustion efficiency decrease caused by lower bed temperature. Decreasing combustion efficiency also causes higher carbon content in the combustor. Thus the reduction rate of NO_x increases (Fig. 11(b)). The SO_2 generation rate from the char depends on its combustion rate, which depends on the temperature, excess air, O_2 concentration, etc. [64]. Although the amount of oxygen increases with increasing excess air, decreasing bed temperature causes a negative effect on coal combustion efficiency and limits the liberation of the fixed sulfur as SO_2. Fig. 11(b) shows the decrease of SO_2 emissions with increasing excess air. Another explanation of decreasing SO_2 and NO_x emissions is the gas dilution caused by increasing excess air.

Fig. 12 shows the effects of bed operational velocity and coal particle diameter on mean bed temperature and emissions of CO, NO_x and SO_2 in modeling results. Fig. 12 plots the predicted model results for three particle diameters (540, 651 and 852 μm) and for six bed operational velocity values (of about 4.15, 4.50, 5.00, 5.50, 6.00 and 6.50 m s^{-1}). For this assumption inlet bed pressure is 1.6 atm and coal feed rate is 7.20 kg h^{-1}.

The bed operational velocity in the combustor is one of the basic design variables of the process. The reason is that with the increase of bed operating velocity the hydrodynamic con-

dition of the combustor changes. As the operational velocity increases particle residence time in the combustor, char combustion rate and bed temperature decreases which results higher CO emission values in flue gases (Fig. 12(a)). Suspension density in the bed decreases with increasing superficial velocity. So, the contact time of NO_x with char particle is reduced, thus reducing the rate of reduction of NO_x. Therefore NO_x emissions increase with the superficial velocity of the combustor. However, it is observed that operational bed velocity has positive effect on SO_2 emission. Particle residence time decreases with decreasing coal particle size and causes lower SO_2 emission formation. This effect is reversed after the value of 5 m s^{-1} (Fig. 12(b)).

As the coal particle size increases, char combustion rate and in consequence bed temperature decreases and this situation causes higher CO concentration in the flue gases (Figs. 11(a) and 12(a)). A smaller mean size of char in the combustor will result in a lower emission of NO_x if other parameters are keep unchanged [35], as clearly seen in Figs. 11(b) and 12(b). However, it is observed that the effect of coal particle size in SO_2 emission is lower than that of NO_x emission. Char combustion rate decreases as the particle diameter increases, and this situation causes lower SO_2 formation in the combustor if Ca/S ratio and limestone particle size are keep unchanged (Fig. 11(a)). As the superficial velocity is concerned it is observed that this tendency is reversed after the value of 5 m s^{-1}. At higher velocities as the residence time of limestone particles is decreased, the sulfur retention decreases in the combustor.

6. Conclusion

In this study, a dynamic 2D model for a CFB combustor has been developed which integrates and simultaneously predicts the hydrodynamics, heat transfer and combustion aspects. The model has been validated against the data from a pilot-scale 50 kW CFB combustor and an industrial-scale 160 MW CFB combustor which uses different types of coal. The model is applicable to wide size range of circulating fluidized bed combustors. Through this model, effects of different operational conditions such as excess air, bed operational velocity and particle diameter on bed temperature and the overall CO, NO_x and SO_2 emissions from the combustor are investigated. The effects of excess air and coal particle diameter on mean bed temperature and emissions of CO, NO_x and SO_2 in modeling results have been investigated for three particle diameters (540, 600 and 750 μm) and for five excess air ratios (of about 20, 40, 60, 80 and 100%). For this assumption inlet bed pressure is 1.2 atm and coal feed rate is 6.48 kg h^{-1}. The effects of bed operational velocity and coal particle diameter on mean bed temperature and emissions of CO, NO_x and SO_2 in modeling results have been investigated for three particle diameters (540, 651 and 852 μm) and for six bed operational velocity values (of about 4.15, 4.50, 5.00, 5.50, 6.00 and 6.50 m s^{-1}). For this assumption inlet bed pressure is 1.6 atm and coal feed rate is 7.20 kg h^{-1}. It is clearly observed that the decreasing bed temperature with excess air and bed operational velocity has a major effect on combustion behavior in small-scale CFB combustors. Bed operational velocity has a more significant effect on CO emission than to bed temperature. Increasing excess air decreases SO_2 and NO_x emissions. However, NO_x emission increases with the operational bed velocity while SO_2 emission decreases.

References

[1] B.J. Harris, J.F. Davidson, Modelling options for circulating fluidized beds: a core/annulus depositions model, in: A.A. Avidan (Ed.), Circulating Fluidized Bed Technology, vol. IV, AIChE Publications, New York, 1994.

[2] K. Smolders, J. Baeyens, Hydrodynamic modelling of the axial density profile in the riser of a low-density circulating fluidized bed, The Canadian Journal of Chemical Engineering 79 (2001) 422–429.

[3] M.R. Hyre, L.R. Glicksman, Axial and lateral solids distribution modeling in the upper region of circulating fluidized beds, Powder Technology 110 (2000) 28–109.

[4] W. Wang, Y. Li, Hydrodynamics simulation of fluidization by using a modified kinetic theory, Industrial and Engineering Chemical Research 40 (2001) 5066–5073.

[5] C.H. Ibsen, T. Solberg, B.H. Hjertager, Evaluation of a three-dimensional numerical model of a scaled circulating fluidized bed, Industrial and Engineering Chemical Research 40 (2001) 5081–5086.

[6] L. Huilin, D. Gidaspow, Hydrodynamics of binary fluidization in a riser: CFD simulation using two granular temperatures, Chemical Engineering Science 58 (2003) 3777–3792.

[7] L.C. Gomez, F.E. Milioli, Numerical study on the influence of various physical parameters over the gas–solid two-phase flow in the 2D riser of a circulating fluidized bed, Powder Technology 132 (2003) 216–225.

[8] M. Koksal, F. Hamdullahpur, CFD simulation of the gas–solid flow in the riser of a circulating fluidized bed with secondary air injection, Chemical Engineering Communications 192 (9) (2005) 1151–1179.

[9] B.G. van Wachem, J.C. Schouten, C.M. van den Bleek, R. Krishna, J.L. Sinclair, Comparative analysis of CFD models of dense gas–solid systems, AIChE Journal 47 (2001) 1035–1051.

[10] P. Basu, Combustion of coal in circulating fluidized-bed boilers: a review, Chemical Engineering Science 54 (1999) 5547–5557.

[11] P. Basu, A. Sett, E.A.M. Gbordzoe, A simplified model for combustion of carbon in a circulating fluidized bed combustor, in: J.P. Mustonen (Ed.), Proceedings of the IX International Conference on Fluidized Bed Combustion, ASME, New York, 1987, pp. 738–742.

[12] I. Heinbockel, F.N. Fett, Simulation of a combined cycle power based on a pressurized circulating fluidized bed combustor, in: P. Basu (Ed.), Heat Recovery System & CHP, vol. 15, n. 2, Pergamon Press, Oxford, 1995, pp. 171–178.

[13] C.G. Remberg, A. Nemet, F.N. Fett, Towards a more general process model for power plants with atmospheric or pressurized fluidized bed combustion, in: F.D.S. Preto (Ed.), Proceedings of the 14th International Conference on Fluidized Bed Combustion, vol. 2, ASME, New York, 1997, pp. 1139–1149.

[14] L. Huilin, Z. Guangbo, B. Rushan, C. Yongjin, D. Gidaspow, A coal combustion model for circulating fluidized bed boilers, Fuel 79 (2000) 165–172.

[15] J. Adanez, P. Gayán, G. Grasa, L.F. de Diego, L. Armesto, A. Cabanillas, Circulating fluidized bed combustion in the turbulent regime: modeling of carbon combustion efficiency and sulfur retention, Fuel 80 (2001) 1405–1414.

[16] Q. Wang, Z. Luo, M. Ni, K. Cen, Particle population balance model for a circulating fluidized bed boiler, Chemical Engineering Journal 93 (2003) 121–133.

[17] Y. Hua, G. Flamant, J. Lu, D. Gauthier, Modelling of axial and radial solid segregation in a CFB boiler, Chemical Engineering and Processing 43 (8) (2003) 971–978.

[18] Y.H. Zhou, H.L. Lu, Y.R. He, Numerical prediction of combustion of carbon particle clusters in a circulating fluidized bed riser, Chemical Engineering Journal 118 (1–2) (2006) 1–10.
[19] T. Knoebig, K. Luecke, J. Werther, Mixing and reaction in the circulating fluidized bed—a three-dimensional combustor model, Chemical Engineering Science 54 (1999) 2151–2160.
[20] T. Hyppanen, Y.Y. Lee, A. Rainio, A three dimensional model for circulating fluidized bed combustion, in: P. Basu, M. Horio, M. Hasatani (Eds.), Circulating Fluidized Bed Technology III, Pergamon Press, Oxford, 1991, pp. 563–568.
[21] Y.P. Tsuo, Y.Y. Lee, A. Rainio, T. Hyppanen, Study of $SO_2/NO_2/N_2O$ emission from CFB boilers with a three-dimensional CFB combustion model, in: M. Kwauk, J. Li (Eds.), Circulating Fluidized Bed Technology V, Science Press, Beijing, 1997, pp. 466–481.
[22] I. Aarna, E.M. Suuberg, The role of carbon monoxide in the NO–carbon reaction, Energy & Fuels 13 (1999) 1145–1153.
[23] I. Aarna, E.M. Suuberg, A review of the kinetics of the nitric oxide–carbon reaction, Fuel 76 (1997) 475–482.
[24] Y.H. Li, G.Q. Lu, V. Rudolph, The kinetics of NO and N_2O reduction over coal chars in fluidized bed combustion, Chemical Engineering Science 53 (1998) 1–7.
[25] H. Aoki, A. Suzuki, Y. Hisaeda, Y. Suwa, T. Nakagawa, M. Yaga, M. Shoji, T. Miura, Recent research and development of combustion simulation, Heat Transfer Asian Research 30 (7) (2001) 581–612.
[26] I.M. Bews, A.N. Hayhurst, S.M. Richardson, S.G. Taylor, The order, Arrhenius parameters, and mechanism of the reaction between gaseous oxygen and solid carbon, Combustion and Flame 124 (2001) 231–245.
[27] R. Abe, H. Sasatsu, T. Harada, N. Misawa, I. Saitou, Prediction of emission gas concentration from pressurized fluidized bed combustion (PFBC) of coal under dynamic operation conditions, Fuel 80 (2001) 135–144.
[28] P. Kilpinen, S. Kallio, J. Konttinen, V. Barisic, Char-nitrogen oxidation under fluidised bed combustion conditions: single particle studies, Fuel 81 (2002) 2349–2362.
[29] H. Liu, B. Feng, J.D. Lu, Coal property effects on N_2O and NO_x formation from circulating fluidized bed combustion of coal, Chemical Engineering Communications 192 (10–12) (2005) 1482–1489.
[30] Y. Zhao, P.Y. Xu, D. Fu, Experimental study on simultaneous desulfurization and denitrification based on highly active absorbent, Journal of Environmental Sciences—China 18 (2) (2006) 281–286.
[31] C. Brereton, Combustion performance, in: A. Avidan, J.R. Grace, T. Knowlton (Eds.), Circulating Fluidized Beds, Blackie Academic & Professional, London, 1997, p. 388.
[32] F. Winter, Single fuel particle and NO_x/N_2O-emission characteristics under circulating fluidized bed combustor conditions, Ph.D. Thesis, University of Technology, Vienna, Austria, 1995.
[33] M. Stenseng, W. Lin, J.E. Johnsson, K.D. Johansen, Modeling of devolatilization in CFB combustion, in: F.D.S. Preto (Ed.), Proceedings of the 14th International Conference on Fluidized Bed Combustion, vol. 1, ASME, New York, 1997, pp. 117–124.
[34] P. Kilpinen, P. Glarborg, M. Hupa, Reburning chemistry at fluidized bed combustion conditions—a kinetic modeling study, Industrial Engineering & Chemistry Research 31 (1992) 1477–1490.
[35] J. Talukdar, P. Basu, A simplified model of nitric oxide emission from a circulating fluidized bed combustor, The Canadian Journal of Chemical Engineering 73 (1995) 635–643.
[36] S. Goel, A. Sarofim, P. Kilpinen, M. Hupa, Emissions of nitrogen oxides from circulating fluidized bed combustors: modeling results using detailed chemistry, in: Proceedings of the 26th International Symposium on Combustion, The Combustion Institute, Naples, 1996.
[37] D. Barletta, A. Marzocchella, P. Salatino, Modelling the SO_2–limestone reaction under periodically changing oxidizing/reducing conditions: the influence of cycle time on reaction rate, Chemical Engineering Science 57 (2002) 631–641.
[38] M.J. Fernandez, H. Kasman, A. Lyngfelt, Methods for measuring the concentrations of SO_2 and gaseous reduced sulphur compounds in the combustion chamber of a circulating fluidized bed boiler, The Canadian Journal of Chemical Engineering 78 (2000) 1138–1144.
[39] N. Eskin, A. Gungor, Numerical computation of a CFB combustor and comparison with experimental results, in: Proceedings of 14th International Conference on Thermal Engineering and Thermogrammetry THERMO, Budapest, Hungary, 2005 (published in a CD).
[40] N. Eskin, A. Gungor, Hydrodynamic simulation of circulating fluidized bed, in: Proceedings of 9th International Research/Expert Conference, Trends in the Development of Machinery and Associated Technology, TMT 2005, Antalya, Turkey, 2005, pp. 673–676.
[41] H. Topal, Experimental investigation of the hydrodynamic, combustion and emission properties of a circulating fluidized bed, Ph.D. Thesis, Gazi University Institute of Science and Technology, Turkey, Gazi University Press, 1999.
[42] A. Gungor, Modeling of circulating fluidized bed combustors, Ph.D. Thesis, Istanbul Technical University Institute of Science and Technology, Turkey, 2006.
[43] A. Svensson, F. Johnsson, B. Leckner, Fluid-dynamics of the bottom bed of circulating fluidized bed boilers, in: Proceedings of XII International Conference on Fluidized Bed Combustion, San Diego, CA, 1993, pp. 887–897.
[44] J. Werther, J. Wein, Expansion behavior of gas fluidized beds in the turbulent regime, AIChE Symposium Series 301 (90) (1994) 31–44.
[45] B. Leckner, M.R. Golriz, W. Zhang, B.A. Andersson, F. Johnsson, Boundary layers first measurement in the 12 MW CFB plant at Chalmers University, in: Eleventh International Conference on Fluidized Bed Combustion, ASME, 1991, pp. 771–776.
[46] D. Montat, T.D. Maggio, 1D two-phase description of the thermal hydraulic behavior of the furnace of E. Huchet 125 MWe CFB boiler, in: Fifth International Conference on CFB, MSR6, Beijing, 1996.
[47] L. Huilin, B. Ruhsan, Y. Lidan, Z. Guangbo, T. Xiu, Numerical computation of a circulating fluidized bed combustor, International Journal of Energy Research 22 (1998) 1351–1364.
[48] M. Horio, Hydrodynamics, in: J.R. Grace, A.A. Avidan, T.M. Knowlton (Eds.), Circulating Fluidized Beds, Blackie Academic & Professional, London, 1992, p. 40.
[49] F.J.A. Martens, Freeboard phenomena in a fluidized bed coal combustor, Delft University of Technology, The Netherlands, Delft University Press, 1996.
[50] S. Mori, C.Y. Wen, Estimation of bubble diameter in gaseous fluidized beds, AIChE Journal 21 (1975) 109–117.
[51] R.R. Rajan, C.Y. Wen, A comprehensive model for fluidized bed coal combustors, AIChE Journal 26 (1980) 642–655.
[52] C.Y. Wen, Y.H. Yu, Mechanics of fluidization, Chemical Engineering Progress Symposium Series 62 (1966) 100–110.
[53] M.J. Rhodes, X.S. Wang, H. Cheng, T. Hirama, Similar profiles of solids flux in circulating fluidized bed risers, Chemical Engineering Science 47 (7) (1992) 1635–1643.
[54] K.M. Luo, Dilute, dense phase and maximum solids–gas transport, Doctoral Dissertation, Illinois Institute of Technology, Chicago, 1987.
[55] C.A. Palmer, E. Tuncali, K.O. Dennen, T.C. Coburn, R.B. Finkelman, Characterization of Turkish coals: a nationwide perspective, International Journal of Coal Geology 60 (2–4) (2004) 85–115.
[56] A. Kucuk, Y. Kadioglu, M.S. Gulaboglu, A study of spontaneous combustion characteristics of a Turkish lignite: particle size, moisture of coal, humidity of air, Combustion and Flame 133 (3) (2003) 255–261.
[57] S. Cetinkaya, Y. Yurum, Oxidative pyrolysis of Turkish lignites in air up to 500 °C, Fuel Processing Technology 67 (3) (2000) 177–189.
[58] P.K. Agarwal, A single particle model for the evolution and combustion of coal volatiles, Fuel 65 (1986) 803–810.
[59] D.R. Gregory, R.F. Littlejohn, A survey of numerical data on the thermal decomposition of coal, The BCURA Monthly Bulletin 29 (6) (1965) 173–179.
[60] R. Loison, R. Chauvin, Pyrolyse rapide du charbon, Chemie et Industrie 91 (1964) 269–274.
[61] D.H. Fine, S.M. Slater, A.F. Sarofim, G.C. Williams, Nitrogen in coal as a source of nitrogen oxide emission from furnaces, Fuel 53 (1974) 120–128.

[62] H.C. Hottel, G.C. Williams, N.M. Nerheim, G.R. Schneider, Burning rate of carbon monoxide, in: Proceedings of the 10th International Symposium on Combustion, The Combustion Institute, Pittsburgh, 1965, pp. 111–117.
[63] E.D. Ducarne, J.C. Dolignier, E. Marty, G. Martin, L. Delfosse, Modelling of gaseous pollutants emissions in circulating fluidized bed combustion of municipal refuse, Fuel 77 (1998) 1399–1410.
[64] J. Adanez, L.F. de Diego, P. Gayan, L. Armesto, A. Cabanillas, Modeling of sulfur retention in circulating fluidized bed combustors, Fuel 75 (3) (1996) 262–270.
[65] J. Hannes, U. Renz, C.M. Van den Bleek, The IEA model for circulating fluidized bed combustion, in: K.J. Heinschel (Ed.), Proceedings of the 13th International Conference on Fluidized Bed Combustion, Orlando, ASME, 1995, pp. 287–296.
[66] F. Bellgardt, F. Hembach, M. Schossler, J. Werther, Modeling of large scale atmospheric fluidized bed combustors, in: J.P. Mustonen (Ed.), Proceedings of the 9th International Conference on Fluidized Bed Combustion, Boston, ASME, 1987, p. 713.
[67] M.J. Rhodes, D. Geldart, The upward flow of gas/solid suspensions, Part 2: A practical quantitative flow regime diagram for the upward flow of gas/solid suspensions, Chemical Engineering Research and Design 67 (1989) 30–37.
[68] Q. Wang, Z. Luo, X. Li, M. Fang, M. Ni, K. Cen, A mathematical model for a circulating fluidized bed (CFB) boiler, Energy 24 (1999) 633–653.
[69] P. Basu, P.K. Nag, Review of heat transfer in high temperature circulating fluidized bed, Chemical Engineering Science 51 (1996) 1–26.
[70] G.A. Ryabov, A.I. Kuruchkin, O.M. Folomeev, Investigation of heat transfer to the water walls on an aerodynamic model of a circulating fluidized-bed boiler, Thermal Engineering 46 (8) (1999) 674–680.
[71] Y.P. Tsuo, D. Gidaspow, Computation of flow patterns in circulating fluidized beds, AIChE Journal 36 (6) (1990) 885–896.
[72] H. Topal, A.T. Atimtay, A. Durmaz, Olive cake combustion in a circulating fluidized bed, Fuel 82 (2003) 1049–1056.
[73] M.A. Field, D.W. Gill, B.B. Morgan, P.W.G. Hawksley, Combustion of pulverized coal, Coal Utilization and Research Association 31 (6) (1967) 285–292.
[74] R.H. Borgwardt, Kinetics of the reaction of SO_2 with calcined limestone, Environmental Science and Technology 4 (1970) 49–57.